^{99m}Tc-hematoporphyrin linked albumin nanoparticles for lung cancer targeted photodynamic therapy and imaging†

Su-Geun Yang,[ab] Ji-Eun Chang,[e] Byungchul Shin,[c] Sanghyun Park,[c] Kun Na[d] and Chang-Koo Shim*[e]

Received 21st May 2010, Accepted 14th July 2010
DOI: 10.1039/c0jm01544j

In this study, we fabricated albumin nanoparticles (ANP) using a solvent diffusion method and modified the surface of the ANP with hematoporphyrin (HP) which has been used for cancer photodynamic therapy. Hematoporphyrin linked albumin nanoparticles (HP-ANP) were further functionalized with gamma-emitting nuclides (^{99m}Tc) for scintigraphic imaging. The fabrication method for HP-ANP was optimized extensively to obtain HP-ANP particles within the size range of 100 to 200 nm. HP-ANP had enhanced accumulation in A549 and CT-26 cancer cell lines, and photodynamic activity against A549 cells after UV exposure. HP-ANP also showed increased accumulation in murine lung tumors, which was induced by CT-26 colon cancer cells, compared to normal lungs. Pharmacokinetics of ^{99m}Tc chelated HP-ANP (^{99m}Tc-HP-ANP) was estimated through scintigraphic imaging of rabbits. ^{99m}Tc-HP-ANP demonstrated good imaging properties in the rabbit with a much more extended biological half life compared to ^{99m}Tc-HP. ^{99m}Tc-HP-ANP could be utilized as a radio-diagnostic tool for cancer as well as the obvious application for photodynamic therapy.

Introduction

Recently nanotechnology has become the cynosure in science and engineering.[1] Nanotechnology combines all areas of science; physics, chemical engineering, material science and medicine *etc.*[2] Scientists are now able to precisely control the size of nano-particles in dimensions of 10, 20, 50 and 100 nm.[3] Interestingly, nanomaterials display totally different physico-chemical and biological properties such as pharmacokinetics, intracellular-trafficking, auto-fluorescence and magnetic properties that cannot be observed in the micro-state.[4]

Nanoparticles, in sizes under 200 nm, demonstrate great potential as drug carriers which penetrate the abnormal neo-vasculature windows and exclusively accumulate into malignant lesions with decreased exposure to other vital organs.[5] This typical property, known as passive targeting, has been utilized for cancer drug targeting.

Recent understanding about cancer biomarkers also enables us to functionalize nanoparticles which can actively travel to the tumor with more enhanced efficiency. Various targeting ligands such as folic acid,[6] cRGD,[7,8] and VEGF antibody[9] *etc.* have been explored as a paddle for nanoparticles. In the near future, nanoparticles could be well-functionalized enough to find, fix or eliminate a single diseased cell in the body, ultimately approaching the definitive goal of nano-therapy.

Nanomaterials have been explored for the diagnosis of cancer.[10] Some materials that exhibit strong fluorescence, like quantum dots, have been developed as a tumor marker after surface-modification with cancer-targeting ligands.[11,12] Another example is imaging-probes such as super-paramagnetic iron oxide (SPIO); gadolinium chelates are loaded on functionalized carriers to increase contrast between tumor and normal tissue.[8,13,14] Application of newly designed nano-imaging probes with improved functionalities becomes more prevalent not only in the diagnosis of cancer but also in image-guided cancer therapy.

However, clinical application of experimental nanomaterials raises great concerns about safety despite their superior performance.[15] Systemic side effects, which suspiciously originate from nanomaterials, have been also reported in many examples such as decreased glomerular filtration rate, immune response and the dreadful accumulation of nanoparticles on central nerve systems *etc.*[16,17] Safety assurance of nanomaterials is getting more imperative to access further clinical trials.

Our research employed albumin and porphyrins to design multifunctional nanoparticles, which are regarded as safe and already approved for clinical applications.[18] Albumin nanoparticles have drawn more attention due to their biocompatibility and wide application for many cancer drugs. The recent clinical success of nanoparticle albumin-bound paclitaxel (Abraxane™) for treatment of metastatic breast cancer widely opened the feasibility of albumin nanoparticles for medical purposes.[19]

Porphyrins have been utilized in various fields stemming from their diverse properties; photodynamic therapy (PDT), chelating agents and cancer diagnostic markers. Porphyrins produce

[a]*Utah-Inha DDS and Advanced Therapeutics, Incheon, 406-840, Republic of Korea. E-mail: Sugeun.Yang@Inah.ac.kr; Fax: +82 32 850 9400; Tel: +82 32 850 9400*
[b]*Clinical Research Center, School of Medicine, Inha University, Incheon, 400-712, Republic of Korea*
[c]*Division of Radioisotope Production and Application, Korea Atomic Energy Research Institute, Daejeon, 305-353, South Korea*
[d]*Department of Biotechnology, The Catholic University of Korea, Bucheon, 420-743, Republic of Korea*
[e]*National Research Laboratory for Transporters Targeted Drug Design, College of Pharmacy, Seoul National University, Seoul, 151-742, Republic of Korea. E-mail: shimck@snu.ac.kr; Fax: +82 2 880 7878; Tel: +82 2 880 7873*
† Electronic supplementary information (ESI) available: Further experimental details. See DOI: 10.1039/c0jm01544j

a singlet oxygen ($^1O_2$) under UV exposure to induce apoptosis of tumor cells.[20–22] Some researchers utilized specific properties of porphyrins (*i.e.*, intrinsic fluorescence and high affinity for neoplastic tissue) for the development of cancer diagnostic markers.[18] Another typical property of porphyrins is chelating power similar to EDTA, in that they form bonds to a metal ion through nitrogen. But PDT has been limited to light penetrable cancers such as oral cavity carcinoma, bronchial cancer and cervical cancer, *etc.*[23] Out-door activities during the therapy are extremely restricted because of the toxicity to skin and the retina under sunlight. More improved targeted design for PDT is needed for decreased toxicity together with enhanced therapeutic efficacy. An increased accumulation of porphyrins at the tumor site may allow PDT for deeper site organs such as lung and liver, although the penetration of UV may be decreased by distance.

In this study we fabricated albumin nanoparticles (ANP) based on a solvent diffusion method,[24] and attached hematoporphyrin (HP) on the surface of ANP for cancer targeting and imaging. Surface morphology, particle size, *in vitro* cellular uptake and *in vivo* cancer targeting of the HP attached albumin nanoparticles (HP-ANP) were evaluated.

Experimental

Materials and methods

Preparation of HP-ANP. HP-ANP was prepared as follows: 250 mg of serum albumin was dissolved in 10.0 ml of purified water. Then, pH was adjusted to be 8.0–8.5 by drops of 0.1 N NaOH, and solvent diffusion was induced by adding 40.0 ml of absolute ethanol at a prefixed feeding rate (1–20 mL min^{-1}) under magnetic stirring. Between 50 and 240 μL of 8% glutaraldehyde was added subsequently to induce cross-linking of albumin. The resulting ANP suspension was magnetically stirred overnight, centrifuged at 1000 rpm for 10 min (5415R, Effendorf, Germany) and resuspended in distilled water or pH 9.7 carbonate buffer at a concentration of 5.0 mg mL^{-1}. Surface-derivatization of ANP was performed by adding N-hydroxysuccinimide ester of HP (HP-NHS) which was prepared according to the reported method (see ESI†).[25] The applied amount of HP-NHS was adjusted to 1.0 to 20.0% of the weight of ANP. The acquired HP-ANP was purified by three cycles of centrifugation (1000 rpm, 10 min) and filtration (0.45 μm).

Characterization of HP-ANP. The particle size and zeta potential of nanoparticles was measured in an aqueous suspension using a dynamic light scattering (DLS) instrument (ELS-8000, Otsuka electronics co., Japan) equipped with a 15 mW laser diode and PMT detector. Samples were appropriately diluted with water for measurement. Scattered light was detected at a 90° angle at room temperature. Zeta potential was calculated from the electrophoretic mobility. TEM images of HP-ANP and ANP were acquired on a JEM 1010 (Jeol Co, Tokyo, Japan). Diluted nanoparticle suspension was dropped on the glow-discharged grid and allowed to stand for drying. Then, the grid was stained with one drop of 2% phosphotungstic acid and introduced to TEM. The optical property of HP-ANP was evaluated using a luminescence spectrometer (LS55, PerkinElmer, USA). Emission spectra of HP, ANP and HP-ANP solution were scanned using an excitation wavelength of 405 nm and 10 nm of band width.

***In vitro* cellular uptake of ANP and HP-ANP.** *In vitro* cellular uptake of ANP and HP-ANP was estimated using A549 (human alveolar epithelial cancer cell line) and CT-26 (murine colon cancer cell line) cells. Five mg of FITC labelled albumin and 245 mg of albumin were employed to make ANP and HP-ANP. In this way, FITC loaded HP-ANP (FITC-HP-ANP) emits green (ex; 494 nm, em; 521 nm) and red (ex; 420 nm, em; 620 nm) fluorescence from FITC and HP, respectively, whereas FITC-ANP emits only green (ex; 494 nm, em; 521 nm) fluorescence. A549 and CT-26 cells routinely grown with RPMI 1640 medium supplemented with 10% FBS, 100 IU mL^{-1} penicillin, 100 mg mL^{-1} streptomycin, and 2 mM L-glutamine in 5% CO_2 humidified air at 37 °C, were seeded on 6-well plates containing 18 mm coverslips at a concentration of 3×10^5 cells/well and grown up to reach 80% confluence. For uptake study, FITC-ANP and FITC-HP-ANP were added to the cell culture media at a particle concentration of 150 μg/well, respectively and incubated for 5 h at 37 °C. Then, cells were washed three times with PBS buffer, fixed and put on slides coated with mounting medium for confocal microscopy (Leica TCS SP2, Leica microsystems, Germany).

Cytotoxicity study. The cytotoxicity of HP-ANP and ANP was evaluated in A549 lung cancer cells. A549 cells were plated in 96-well plates with a seeding density of 500 cells per well and treated with nanoparticles at a concentration of 50 μg per well 24 h after seeding. Cells were incubated with nanoparticles for 5 h, washed with fresh media and then exposed to UV illumination for 10 min. The amount of ATP in the cells was measured from the luminescent signal, which was produced by the luciferase-catalyzed reaction between luciferin and cellular ATP, using a luminescent counter (Spectra Max M5, Molecular devices, CA) after 2 days of treatment. Cell viability was calculated based on the viability of untreated cells.

^{99m}Tc labelling of HP-ANP and imaging of pharmacokinetics. *In vivo* pharmacokinetics and imaging property of HP-ANP were evaluated on a planar gamma camera (Diacam LC 75-005, Siemens AG, German) after radio-labelling HP with ^{99m}Tc-pertechnetate. Radio-labelling was processed based on the reported method (ESI†).[26] The estimated labelling efficiency of ^{99m}Tc by thin layer chromatography was over 95.0% (Figure S3, ESI†). ^{99m}Tc labelled HP-ANP (^{99m}Tc-HP-ANP) and ^{99m}Tc labelled HP (^{99m}Tc-HP), respectively, were administered to New Zealand white female rabbits through the ear vein at a dose of 0.7 mCi. Rabbits were anaesthetized with an intramuscular injection of ketamine hydrochloride (50 mg ml^{-1} each), placed on the imaging platform, and fixed on a board in anterior position for imaging.

Tumor targeting of HP-ANP. Cancer targeting of HP-ANP was investigated using a murine metastatic lung cancer model. The lung metastasis was induced by tail vein injection of CT-26 cells, a transplantable mouse colon cancer cell line, to CDF1 mice at a concentration of 1×10^5 cells/mouse. The study was conducted 2 weeks after the cell injection after confirming lung

tumor formation through histological examination (Figure S6, ESI†). FITC-ANP and FITC-HP-ANP were injected *via* the tail vein at a dose of 10 mg kg^{-1}. Lungs were harvested at pre-determined time-points after the injection, washed twice with physiological saline, dried with blotting paper and then homogenized for 5 min in an ice bath with 4 times the volume of water using a tissue homogenizer (T25 basic, IKA, Germany). The lung homogenate was extracted twice with 2 mL of ethyl acetate each time. The ethyl acetate fractions were pooled, dried under nitrogen gas and reconstituted with pH 7.0 phosphate buffer for fluorescence spectrophotometry. The accumulation of nanoparticles was estimated based on area under the curve (AUC) of lung concentration which was determined based on the pre-obtained calibration curve.

Results and discussion

The objective of our study was to prove the targeting and imaging property of hematoporphyrin-linked albumin nanoparticles (HP-ANP), which could be applied for further development of visible photodynamic therapy and radio imaging of cancer (Fig. 1A). ANP were prepared by ethanol diffusion techniques.

Variable parameters for the preparation of HP-ANP such as pH of the albumin solution, ethanol feeding rate, the applied amount of HP and glutaraldehyde were explored to obtain nanoparticles within the size range of 100 to 200 nm. Fig. 1B, 1C and S1 (ESI†) show ANP and HP-ANP have spherical shape with narrow particle size distribution.

HP-ANP displayed swollen and rough surfaces with increased size in comparison with ANP (Fig. S1, ESI†). Particle size highly affects *in vivo* organ distribution and cancer targeting efficiency of nanoparticles.[27,28] Optimal size for cancer targeting is known to be around 50–150 nm, in which nonspecific elimination of particles by the liver, spleen and kidney is reduced, whereas

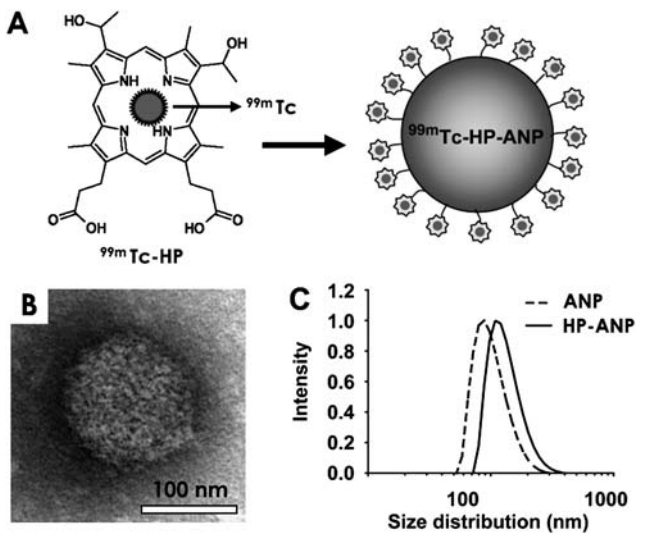

Fig. 1 A) Schematic illustration of ^{99m}TC chelated hematoporphyrin (left) and hematoporphyrin (HP) attached albumin nanoparticles (ANP) for use as a cancer targeting agent (right). B) TEM image of a representative HP-ANP after negative staining with 2% PTA solution. C) Particle size distribution of ANP (dashed line) and HP-ANP (solid line).

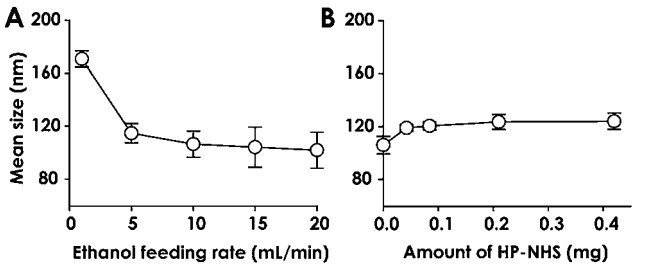

Fig. 2 Controlled particle size of ANP and HP-ANP ($n = 3$, mean ± s.d.). A) Mean particle size of ANP by ethanol feeding rate during solvent diffusion process. B) Mean particle size of HP-ANP after HP-derivatization of ANP. The applied amount of HP-NHS per 1 mg of ANP is shown.

accumulation in the tumor is increased. Fig. 2A shows how ethanol feeding affects the particle size of ANP. Particle sizes around 220 nm were achieved at ethanol feeding of 1 mL min^{-1}.

Particle size decreased to 130 nm as the feeding rate increased. However recovery of ANP dropped below 40.0% when the feeding rate was increased (data not shown). The amount of HP added also affected size of ANP (Fig. 2B). Zeta potential was slightly affected by the HP-derivatization. The estimated zeta potential of ANP was −32.5 mV and changed to −38.3 mV after HP-derivatization. The zeta potential of ANP was comparable with the reported values, and the altered zeta potential of HP-ANP also suggested the successful derivatization of ANP.[29] Sequential experiments proved other factors such as magnetic stirring rate and pH of solution also affected the particle size of ANP (data not shown). Generally, the particle size decreased as the stirring rate increased. Severe aggregation of ANP was observed when the pH of albumin solution was under 8.0 or over 9.0, thus the pH of the albumin solution was precisely controlled to be 8.3. Excess amounts of aldehyde caused particle aggregation, resulting in poor polydispersity and low recovery of particles (data not shown).[24] The optimal amount of glutaraldehyde was determined to be 0.5–0.7 μL per 1 mg of albumin based on the residual amount of free amino groups of albumin, which was estimated using the trinitrobenzene sulfonic acid (TNBS) method (ESI†).[30] The total amount of free amino groups was 507 μmol per gram of albumin. 60% Of amino groups were cross-linked after aldehyde treatment. HP-NHS was attached to about 30% of the residual amino groups (Fig. S2, ESI†). In this condition, the acquired particles were apparently spherical with diameters less than 120 nm, as shown in Fig. 1.

HP and HP-ANP solution exhibited fluorescence emission at 613 and 618 nm, respectively (Fig. 3). A slight red shift of the emission spectrum of HP-ANP suggests a formation of chemical bonding between protein amine and carboxylic acid of HP.

Confocal fluorescence images of A549 and CT-26 cells are shown in Fig. 4. Absence of cell associated fluorescence of CT-26 and A549 cell line (Fig. 4A and 4D) in contrast to an intense cell-associated green and red fluorescence for HP-ANP (Fig. 4B, 4C, 4E and 4F) reveals dependence of nanoparticle uptake on HP conjugation. Using another method, the recovered cells were lysed with 1% TritonX-100 and introduced to an LS55 luminescence spectrometer (Perkin-Elmer, PerkinElmer, USA) to estimate the uptake rate. Uptake of HP-ANP reached a plateau after 5 h of incubation. The uptake rate was so slow that no

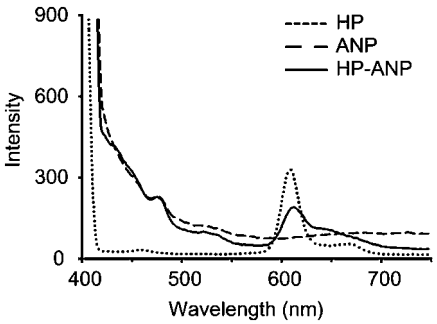

Fig. 3 Emission fluorescence of HP, ANP and HP-ANP using excitation at 405 nm. Bandwidth and scanning speed was 10 nm and 200 nm min^{-1}, respectively.

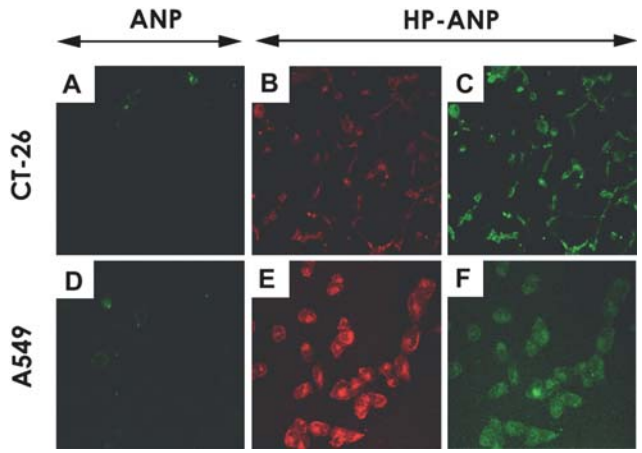

Fig. 4 Uptake of ANP (A and D) and HP-ANP (B, C, E and F) by CT-26 murine colon cancer cells and A549 human lung cancer cells after 5 h exposure. ANP and HP-ANP were fabricated with 5% content of FITC-albumin. Red and green fluorescence were observed from excitation of HP and FITC at 405 and 490 nm, respectively.

significant uptake of HP-ANP was observed after 2 h of incubation.

Bohmer *et al.* observed temperature-dependent cellular uptake of porphyrins and suggested an energy-dependent pathway to explain the uptake mechanism of porphyrins.[31] They found the cellular uptake of porphyrins was delayed up to 5 h before reaching a plateau. Other studies also proved that carrier mediated uptake of porphyrins with saturation kinetics was strongly restrained by inhibitor and low temperature.[32] Shibata *et al.* suggested that porphyrin is taken-up by LDL receptors which are abundantly over-expressed in cancer cells such as glioma cells *etc.*[33] 5-Aminolevulic acid ester (ALA) which is a bio-precursor of prophyrin has been widely studied for use in photodynamic therapy. Some researchers suggested ALA is taken-up *via* peptide transporters,[34] but others have proposed the GABA pathway.[34] The uptake mechanism of porphyrins appears to be distinctive for each cell type and still not fully understood yet. However, porphyrins are generally regarded as an active targeting moiety and are clinically used for cancer therapy which solidifies the proof of their therapeutic potential.

Photodynamic effects of HP-ANP were investigated using A549 human lung cancer cells (Fig. 5). The viability of A549 dropped when the cells were treated with both UV and HP-ANP. UV-nontreated cells, which were treated only with HP-ANP, maintained the same viability as control cells. This study suggests HP-ANP is working as photodynamic therapy and is relatively non-toxic without UV-exposure.

Fig. 5 also shows 5% is the most optimal level for HP derivatization for effective toxicity. This observation corresponds with previous results, which demonstrated that over 5% of HP did not influence the residual amount of free amino-groups (Fig. S2, ESI†) and particle size (Fig. 2).

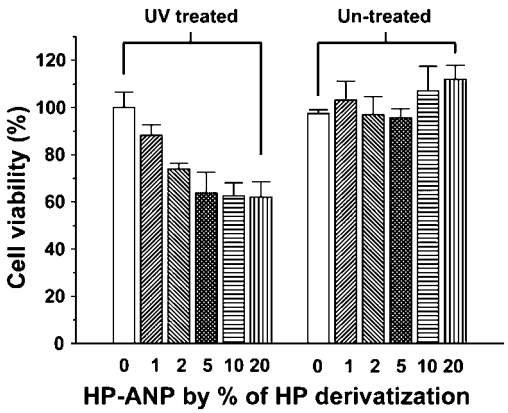

Fig. 5 Cell viability of UV-treated and untreated A549 lung cancer cells after uptake of HP-ANP. Cells were treated with 50 ug/well concentration of HP-ANP for 5 h, washed with media and exposed to UV light. Cell viability was estimated by measuring cellular content of ATP 3 days after treatment.

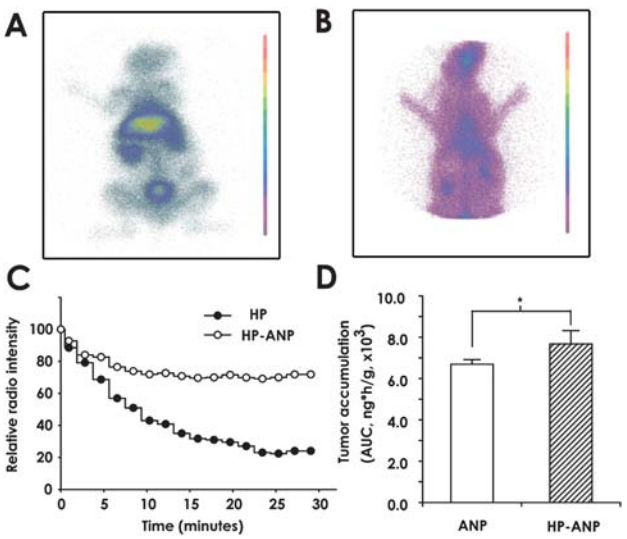

Fig. 6 Pharmacokinetic behaviors of radio-labelled HP-ANP and ANP. *In vivo* rabbit scinti-images after IV injection of ^{99m}Tc-HP-ANP (A) and ^{99m}Tc-HP (B) at a dose of 0.7 mCi. Images were taken 30 min after injection. C) Time dependent radio-intensity of ^{99m}Tc-HP-ANP and ^{99m}Tc-HP, which was estimated by Image J on the basis of scinti-images (Fig. S4, ESI†). D) Accumulation of ANP and HP-ANP on CT-26 murine metastatic lung ($n = 3$, * $P < 0.05$).

Representative rabbit-body scinti-images for two preparations are shown in Fig. 6A and 6B, which are taken 30 min after dosing. The intensity of scinti-images was estimated by Image J and time dependent intensity profiles are shown in Fig. 6C. ^{99m}Tc-HP-ANP showed very different *in vivo* pharmacokinetic properties than ^{99m}Tc-HP, which spread throughout the body instantaneously after dosing and was excreted rapidly *via* the kidneys (Fig. S5, ESI†). ^{99m}Tc-HP-ANP showed much more extended terminal half life ($t_{1/2}$, 16 min) in comparison to ^{99m}Tc-HP (245 min). These results indicate that nano-formulation greatly affected the retention of HP.

Fig. 6D shows the increased accumulation (AUC) of HP-ANP in mouse lung cancer, which was induced by CT-26 murine colon cancer cell, by 14.7% in comparison with ANP ($n = 3$, $P < 0.05$). Increased accumulation of HP-ANP in the lung tumor suggests that HP-ANP might be a good candidate for further therapeutic challenges such as photodynamic therapy for lung tumors. Another potential application of HP is in metal-isotope chelation. As shown in our study, ^{99m}Tc-HP-ANP displayed good imaging properties in the radio-scintiimage study. Especially short half-life gamma emitters like ^{57}Co, ^{111}In and ^{64}Cu *etc.*, which have been used for cancer therapy and imaging, could be applied to HP-ANP for tumor detection and imaging through positron emission tomography (PET).[26,35,36]

Conclusion

In this study, we illustrated the possible application of HP-ANP for cancer targeted imaging and therapy. ANP particles 100–150 nm in size were acquired using a solvent diffusion method. HP-ANP showed enhanced uptake by cancer cell lines (A549 and CT-26) and higher accumulation in a murine lung cancer model. Photodynamic activity of HP-ANP was proved after UV exposure using A549 lung cancer cells. Radio-labelled HP-ANP showed good radio-scintiimages in a rabbit, which was enough to see the body retention and organ distribution. The increased targeting efficiency of HP-ANP, which is endowed by nano-design and HP-modification, allows further development of nano-carriers for cancer photodynamic therapy and radio imaging.

Acknowledgements

This work was supported by International R&D Center START-UP FUND Program funded by Incheon Free Economic Zone Authority (IFEZA) and Ministry of Knowledge and Economy (MKE), and a grant from the Korean Ministry of Science and Technology through the National Research Laboratory Program (ROA-2006-000-10290-0) and

References

1 D. Peer, J. M. Karp, S. Hong, O. C. Farokhzad, R. Margalit and R. Langer, *Nat. Nanotechnol.*, 2007, **2**, 751–760.
2 L. Zhang, F. X. Gu, J. M. Chan, A. Z. Wang, R. S. Langer and O. C. Farokhzad, *Clin Pharmacol Ther*, 2007, **83**, 761–769.
3 W. H. De Jong, W. I. Hagens, P. Krystek, M. C. Burger, A. J. Sips and R. E. Geertsma, *Biomaterials*, 2008, **29**, 1912–1919.
4 P. K. Jain, X. Huang, I. H. El-Sayed and M. A. El-Sayed, *Acc. Chem. Res.*, 2008, **41**, 1578–1586.
5 S. D. Perrault, C. Walkey, T. Jennings, H. C. Fischer and W. C. Chan, *Nano Lett.*, 2009, **9**, 1909–1915.
6 E. I. Galanzha, E. V. Shashkov, T. Kelly, J. W. Kim, L. Yang and V. P. Zharov, *Nat. Nanotechnol.*, 2009, **4**, 855–860.
7 J. D. Hood, M. Bednarski, R. Frausto, S. Guccione, R. A. Reisfeld, R. Xiang and D. A. Cheresh, *Science*, 2002, **296**, 2404–2407.
8 J. S. Guthi, S. G. Yang, G. Huang, S. Li, C. Khemtong, C. W. Kessinger, M. Peyton, J. D. Minna, K. C. Brown and J. Gao, *Mol. Pharmaceutics*, 2010, **7**, 32–40.
9 D. H. Yu, Q. Lu, J. Xie, C. Fang and H. Z. Chen, *Biomaterials*, 2010, **31**, 2278–2292.
10 E. K. Pauwels and P. Erba, *Drug News Perspect.*, 2007, **20**, 213–220.
11 K. C. Weng, C. O. Noble, B. Papahadjopoulos-Sternberg, F. F. Chen, D. C. Drummond, D. B. Kirpotin, D. Wang, Y. K. Hom, B. Hann and J. W. Park, *Nano Lett.*, 2008, **8**, 2851–2857.
12 X. Gao, Y. Cui, R. M. Levenson, L. W. Chung and S. Nie, *Nat. Biotechnol.*, 2004, **22**, 969–976.
13 N. Nasongkla, E. Bey, J. Ren, H. Ai, C. Khemtong, J. S. Guthi, S. F. Chin, A. D. Sherry, D. A. Boothman and J. Gao, *Nano Lett.*, 2006, **6**, 2427–2430.
14 S. D. Swanson, J. F. Kukowska-Latallo, A. K. Patri, C. Chen, S. Ge, Z. Cao, A. Kotlyar, A. T. East and J. R. Baker, *Int. J. Nanomedicine*, 2008, **3**, 201–210.
15 M. A. Maurer-Jones, K. C. Bantz, S. A. Love, B. J. Marquis and C. L. Haynes, *Nanomedicine*, 2009, **4**, 219–241.
16 G. Bhabra, A. Sood, B. Fisher, L. Cartwright, M. Saunders, W. H. Evans, A. Surprenant, G. Lopez-Castejon, S. Mann, S. A. Davis, L. A. Hails, E. Ingham, P. Verkade, J. Lane, K. Heesom, R. Newson and C. P. Case, *Nat. Nanotechnol.*, 2009, **4**, 795–796.
17 A. El-Ansary and S. Al-Daihan, *J. Toxicol.*, 2009, **2009**, 754810.
18 K. Berg, P. K. Selbo, A. Weyergang, A. Dietze, L. Prasmickaite, A. Bonsted, B. O. Engesaeter, E. Angell-Petersen, T. Warloe, N. Frandsen and A. Hogset, *J. Microsc.*, 2005, **218**, 133–147.
19 M. R. Green, G. M. Manikhas, S. Orlov, B. Afanasyev, A. M. Makhson, P. Bhar and M. J. Hawkins, *Ann. Oncol.*, 2006, **17**, 1263–1268.
20 R. Hornung, M. K. Fehr, J. Monti-Frayne, T. B. Krasieva, B. J. Tromberg, M. W. Berns and Y. Tadir, *Photochem. Photobiol.*, 1999, **70**, 624–629.
21 A. M. Gloi and E. Beck, *Vet Ther*, 2003, **4**, 155–165.
22 E. B. Elmer, W. C. Wood, A. M. Cohen and M. Bamberg, *J. Surg. Oncol.*, 1987, **34**, 113–119.
23 H. I. Pass, *J. Natl. Cancer Inst.*, 1993, **85**, 443–456.
24 K. Langer, S. Balthasar, V. Vogel, N. Dinauer, H. von Briesen and D. Schubert, *Int. J. Pharm.*, 2003, **257**, 169–180.
25 L. Zhang, S. Hou, S. Mao, D. Wei, X. Song and Y. Lu, *Int. J. Pharm.*, 2004, **287**, 155–162.
26 A. K. Babbar, A. K. Singh, H. C. Goel, U. P. Chauhan and R. K. Sharma, *Nucl. Med. Biol.*, 2000, **27**, 587–592.
27 K. Sato, D. Krag, K. Tamaki, M. Anzai, H. Tsuda, S. Kosuda, S. Kusano, H. Hiraide and H. Mochizuki, *Breast Cancer*, 2004, **11**, 256–263.
28 M. P. Desai, V. Labhasetwar, E. Walter, R. J. Levy and G. L. Amidon, *Pharm. Res.*, 1997, **14**, 1568–1573.
29 Y. Mo, M. E. Barnett, D. Takemoto, H. Davidson and U. B. Kompella, *Mol Vis*, 2007, **13**, 746–757.
30 C. Weber, C. Coester, J. Kreuter and K. Langer, *Int. J. Pharm.*, 2000, **194**, 91–102.
31 R. M. Bohmer and G. Morstyn, *Cancer Res*, 1985, **45**, 5328–5334.
32 C. J. Carrano, M. Tsutsui and S. McConnell, *Chem.-Biol. Interact.*, 1978, **21**, 233–248.
33 Y. Shibata, A. Matsumura, F. Yoshida, T. Yamamoto, K. Nakai, T. Nose, I. Sakata and S. Nakajima, *Cancer Lett.*, 2001, **166**, 79–87.
34 L. Rodriguez, A. Batlle, G. Di Venosa, S. Battah, P. Dobbin, A. J. Macrobert and A. Casas, *Br. J. Pharmacol.*, 2006, **147**, 825–833.
35 J. C. Roberts, S. D. Figard, J. A. Mercer-Smith, Z. V. Svitra, W. L. Anderson and D. K. Lavallee, *J. Immunol. Methods*, 1987, **105**, 153–164.
36 H. T. Whelan, L. H. Kras, K. Ozker, D. Bajic, M. H. Schmidt, Y. Liu, L. A. Trembath, F. Uzum, G. A. Meyer, A. D. Segura and B. D. Collier, *J. Neuro-Oncol.*, 1994, **22**, 7–13.

